Fabry–Perot diaphragm fiber-optic sensor

Ken K. Chin,[1,*] Yan Sun,[2] Guanhua Feng,[1] George E. Georgiou,[1] Kangzhu Guo,[3] Edip Niver,[4] Harry Roman,[5] and Karen Noe[5]

[1]Department of Physics, New Jersey Institute of Technology, Newark, New Jersey 07102, USA
[2]Materials Science and Engineering Program, New Jersey Institute of Technology, Newark, New Jersey 07102, USA
[3]Department of Physics, Rutgers University–Newark Campus, Newark, New Jersey 07102, USA
[4]Department of Electrical and Computer Engineering, New Jersey Institute of Technology, Newark, New Jersey 07102, USA
[5]Public Service Enterprise Group Services Corporation, 80 Park Plaza, Newark, New Jersey 07101, USA

*Corresponding author: chin@njit.edu

Received 27 June 2007; accepted 20 July 2007;
posted 7 September 2007 (Doc. ID 80273); published 23 October 2007

The general theory of a diaphragm fiber-optic sensor (DFOS) is proposed. We use a critical test to determine if a DFOS is based on Fabry–Perot interference or intensity modulation. By use of the critical test, this is the first design, to the best of our knowledge, of a purely Fabry–Perot DFOS, fabricated with microelectromechanical system technology, and characterized as an audible microphone and ultrasonic hydrophone with orders of improvement in signal-to-noise ratio. © 2007 Optical Society of America

OCIS codes: 060.0060, 060.2370, 060.2340.

1. Introduction

In recent years there has been intense effort to develop a new diaphragm fiber-optic sensor (DFOS). The DFOS [1–7] shown in Fig. 1, uses a diaphragm as the sensing element to detect pressure or acoustic wave disturbance and an optical fiber to deliver the steady or modulated probe light as well as to receive the reflected light modulated by signals under detection. In addition to its small size, low cost, flexibility, high sensitivity, convenience for multiplexing and array integration, and versatility of its diaphragm fiber structure, the DFOS is resistant to electromagnetic interference.

2. Theory of the Diaphragm Fiber-Optic Sensor

Two mechanisms are responsible for the DFOS to perform as a pressure or acoustic sensor: interference and intensity. The interference-based mechanism is described by the Fabry–Perot interference of multiply reflected beams between the two surfaces of the gap (Fig. 2). The sum of the fields of multiply reflected beams of a normally incident beam with an unity field is

$$E^{(r)} = r + tt'r''e^{i2\phi}\left[1 + \left(r'r''e^{i2\phi}\right) + \left(r'r''e^{i2\phi}\right)^2 + \cdots\right], \tag{1}$$

where r, r', r'', t, and t' are the reflection and transmission coefficients of the interfaces shown in Fig. 2, and

$$\phi = (2n\pi L/\lambda) \tag{2}$$

is the phase shift that is due to propagation of the beam of wavelength λ through the interference gap of width L and refractive index n. Assuming that there is no loss at the interfaces, the ratio of the output or reflected optical power versus the input or incident power of a Fabry–Perot interferometric device is

$$\frac{I^{(o)}}{I^{(i)}} = \frac{E^{(r)}E^{(r)*}}{E^{(i)}E^{(i)*}} = \left(r + \frac{tt'r''e^{i\phi}}{1 - r'r''e^{i\phi}}\right)\left(r + \frac{tt'r''e^{-i\phi}}{1 - r'r''e^{-i\phi}}\right) = \frac{2R_a - 2R_g\cos\phi}{1 + R_g{}^2 - 2R_g\cos\phi}. \tag{3}$$

0003-6935/07/317614-06$15.00/0
© 2007 Optical Society of America

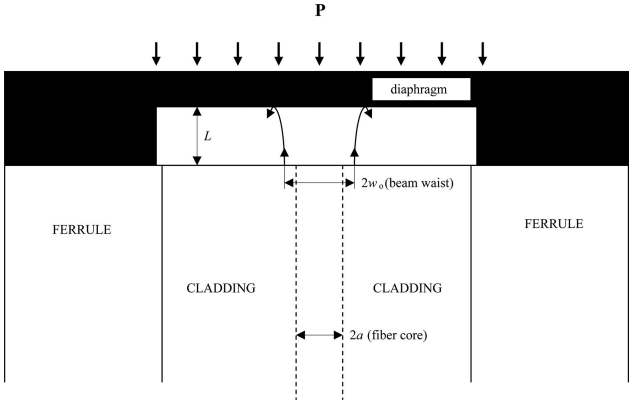

Fig. 1. Principle of the DFOS.

We define the geometric mean reflectance R_g of the two interfaces n/n' and n/n'' by

$$R_g = |r'r''|, \tag{4}$$

and the arithmetic mean reflectance R_a of the two interfaces n/n' and n/n'' by

$$R_a = \frac{r'^2 + r''^2}{2}. \tag{5}$$

When the two sides of the interference gap are the same medium, then $r' = r''$ and the geometric and arithmetic mean reflectance becomes equal, i.e., $R_a = R_g = R$. We can have Eq. (3) expressed in the well-known form associated with an Airy function:

$$\frac{I^{(o)}}{I^{(i)}} = \frac{2R - 2R\cos\phi}{1 + R^2 - 2R\cos\phi} \tag{6}$$

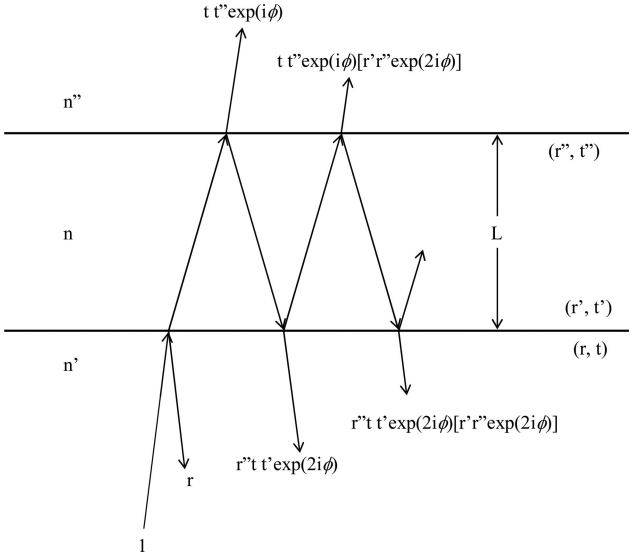

Fig. 2. Plane wave Fabry–Perot interferometric device with the incident beam tilted for convenience of illustration.

and its harmonic approximation [8,9]

$$\frac{I^{(o)}}{I^{(i)}} \approx F\sin^2\frac{\phi}{2} = \frac{F}{2}(1 - \cos\phi) = \frac{F}{2}\left[1 - \cos\left(\frac{4\pi n}{\lambda}L\right)\right], \tag{7}$$

where finesse F, defined by

$$F = \frac{4R}{(1-R)^2}, \tag{8}$$

is smaller than 0.2. Note that Eq. (7) is the expression of two-beam interference with an attenuation coefficient of $F/2$.

When used as a pressure or acoustic sensor, under the condition of small deflection ($\Delta L < 0.1h$), from the theory of plate [10] we have deflection ΔL of the center of the diaphragm expressed as a linear function of pressure P under measurement [10,11]

$$\Delta L = L - L_o = \frac{b^4(1-\nu^2)}{\eta E h^3}P, \tag{9}$$

where b is the size of the edge-clamped diaphragm, h is the thickness of the diaphragm, E and ν are the Young's modulus and Poisson ratio of the diaphragm material, respectively, and η is a constant that depends on the shape of the diaphragm. Substituting Eqs. (9) and (2) into Eqs. (3) and (7), we have

$$\frac{I^{(o)}}{I^{(i)}} = \frac{2R_a + 2R_g\sin\left(\frac{\pi}{2P_o}P + \theta_o\right)}{1 + R_g{}^2 + 2R_g{}^2\sin\left(\frac{\pi}{2P_o}P + \theta_o\right)}, \tag{10}$$

$$\frac{I^{(o)}}{I^{(i)}} \approx \frac{F}{2}\left[1 + \sin\left(\frac{\pi}{2P_o}P + \theta_o\right)\right], \tag{11}$$

respectively, where

$$P_o = \frac{\eta E h^3 \lambda}{8b^4(1-\nu^2)n}, \tag{12}$$

and θ_0 determines the so-called quadrant or Q point, ideally adjusted and stabilized to be zero for maximum dynamic range and minimum harmonic distortion of the sensor. Equations (3) and (7), as well as Eq. (10) and approximation (11), are widely quoted as the basis of the newly developed DFOS, usually dubbed with the epithet of Fabry–Perot.

A question arises: under what condition and to what extent can plane wave approximation that is manifest in Eq. (3) be adapted to the light that is delivered by a fiber, multiply reflected by a flat diaphragm and fiber surfaces, and coupled back to the same fiber? Without losing generality, we present our analysis for the case of a weakly guided step-index

single-mode fiber. It is well known that the Bessell–Kapteyn function or the analytic solution of the fundamental HE_{11} mode of single-mode fiber is also accurately (greater than 99.5% accuracy) approximated by a Gaussian distribution of a transverse and linearly polarized electric field [12,13],

$$E_x = \left(\frac{4\sqrt{\mu_o/\varepsilon_o}P}{\pi n_2 w_o^{\,2}}\right)^{1/2} \exp\left(-\frac{r^2}{w_o^{\,2}}\right) e^{i\beta z}, \tag{13}$$

and magnetic field

$$H_y = \frac{E_x}{\sqrt{\mu/\varepsilon}} = \left(\frac{4n_2\sqrt{\varepsilon_o/\mu_o}P}{\pi w_o^{\,2}}\right)^{1/2} \exp\left(-\frac{r^2}{w_o^{\,2}}\right) e^{i\beta z}, \tag{14}$$

where P is the transmitted rms (root mean square) power of the HE_{11} mode beam and w_o is the waist of the Gaussian beam that can be calculated with the empirical formula [14]

$$\frac{w_o}{a} = 0.65 + \frac{1.619}{V^{3/2}} + \frac{2.879}{V^6}. \tag{15}$$

When the guided HE_{11} mode light exits the fiber endface into free space in the $x'y'z'$ coordinate system, under the condition that no power is reflected or lost, the beam keeps the Gaussian distribution of its electric and magnetic fields at the interface and propagates approximately as the Gaussian beam with an angular divergence and gradual phase shift:

$$E_{x'} = \left(\frac{4\sqrt{\mu_o/\varepsilon_o}P}{\pi w^2}\right)^{1/2} \exp\left(-\frac{r'^2}{w^2}\right) e^{ikz'} e^{\frac{ikr'^2}{2R(z')}} e^{-i\eta(z')}, \tag{16}$$

where

$$w = w(z') = w_o\sqrt{1 + \left(\frac{z'}{z_o}\right)^2}, \tag{17}$$

$$R = R(z') = z'\left(1 + \frac{z_o^{\,2}}{z'^2}\right), \tag{18}$$

$$\eta(z') = \tan^{-1}\frac{z'}{z_o} \tag{19}$$

are the beam width, beam spherical wavefront radius, and Guoy phase shift after the beam propagates a distance z'. In Eq. (17)

$$z_o = \left(\pi w_o^{\,2}/\lambda\right) \tag{20}$$

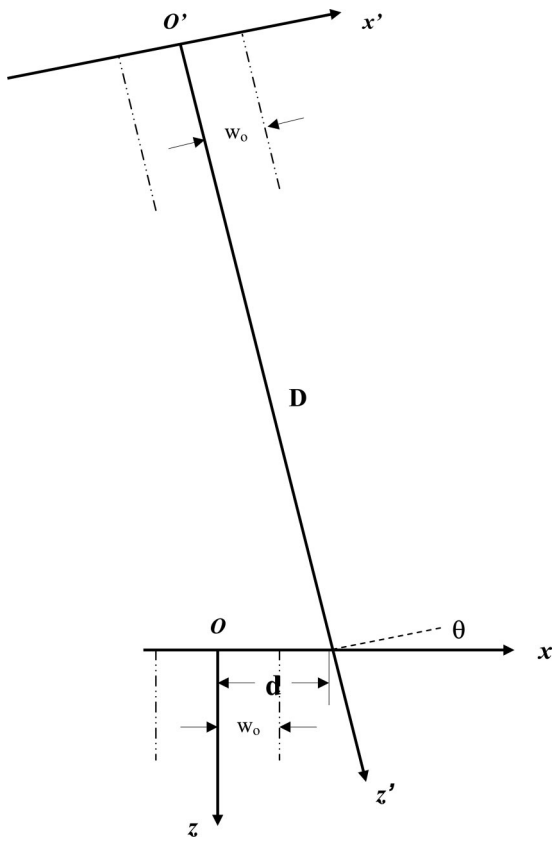

Fig. 3. Gaussian beam emitted from fiber O' coupled into fiber O with longitudinal, lateral, and angular mismatches of D, d, and θ.

is the Rayleigh length of the Gaussian beam, which signifies the angular spread of the beam:

$$\theta_o = \lim_{z'\to\infty} \tan^{-1}\frac{w(z')}{z'} = \tan^{-1}\frac{w_o}{z_o} \approx \frac{w_o}{z_o}. \tag{21}$$

Assume that the fiber at O' in the $x'y'z'$ coordinate system emits a Gaussian beam, which is coupled into the same kind of fiber at O in the xyz coordinate system as another Gaussian beam. The two fibers can undergo a longitudinal, lateral, and angular misalignment of D, d, and θ, respectively, which is equivalent to the two Gaussian beams having the same mismatches (Fig. 3). Then

$$y' = y, \tag{22}$$

$$z' = z\cos\theta + (x - d)\sin\theta + D, \tag{23}$$

$$x' = -z\sin\theta + (x - d)\cos\theta. \tag{24}$$

The coupling coefficient or efficiency of the optical power coupling is

$$T = \left[\frac{1}{P}\frac{1}{2}\,\mathrm{Re}\left(\int_0^\infty E_x^{\,*} H_y 2\pi r\,dr\right)\right]^2, \tag{25}$$

where

$$E_x = E_{x'} \cos\theta = \cos\theta\left(\frac{4\sqrt{\mu_o/\varepsilon_o}P}{\pi w^2}\right)^{1/2} \times \exp\left(-\frac{r'^2}{w^2}\right) e^{ikD} e^{\frac{ikr'^2}{2R\langle z'\rangle}} e^{-i\eta(z')}, \tag{26}$$

a free-space Gaussian beam, is the approximate solution of the Maxwell equations, and

$$H_y = \frac{E_x}{\sqrt{\mu_o/\varepsilon_o}} = \left(\frac{4\sqrt{\varepsilon_o/\mu_o}P}{\pi w_o^{\,2}}\right)^{1/2} \exp\left(-\frac{r^2}{w_o^{\,2}}\right) e^{i\beta z} \tag{27}$$

is the Gaussian approximation of the Bessel–Kapteyn function of the same power as in Eq. (26). Substituting Eqs. (26) and (27), into Eq. (25), utilizing

$$r^2 = x^2 + y^2, \qquad r'^2 = x'^2 + y'^2 \tag{28}$$

and neglecting higher-order terms, we have

$$T = \left(\frac{2w_o w'}{w_o^{\,2} + w'^2}\right)^2 \exp\left(-\frac{2d^2}{w_o^{\,2} + w'^2}\right) \exp\left[-\frac{2(\pi w_o w'\theta)^2}{(w_o^{\,2} + w'^2)\lambda^2}\right], \tag{29}$$

which essentially is the product of the three well-known results of Marcuse [14] of fiber coupling efficiency when there is longitudinal, lateral, or angular misalignment.

By use of an embossed center, the DFOS has virtually no lateral misalignment. It, however, must have a gap of width L, which is essential for a DFOS to sense by use of diaphragm deflection, as well as an angular misalignment of α, which is difficult to avoid completely. As shown in Fig. 4, by use of mirror symmetry and imaging, the Gaussian beam emitted from fiber source O, after being reflected once by the diaphragm, is treated as from its image O' for the calculation of coupling coefficient $T^{(1)}$. After being reflected twice by the diaphragm, the Gaussian beam emitted from fiber source O is treated as from its image O'' for the calculation of coupling coefficient $T^{(2)}$. Obviously, $T^{(0)} = 1$, since the HE_{11} mode couples back into itself without loss. Neglecting higher-order terms, with respect to O, O' has a longitudinal, angular, and lateral mismatch. After reflected by the diaphragm m times, the misalignments are

$$D_m = 2mL, \tag{30}$$

$$\theta_m = 2m\alpha, \tag{31}$$

$$d_m = 2m^2\alpha L. \tag{32}$$

The fiber coupling coefficients $T^{(m)}$ after they mth reflection from the diaphragm can be calculated by substituting Eqs. (30), (31), and (32) into Eq. (29). If

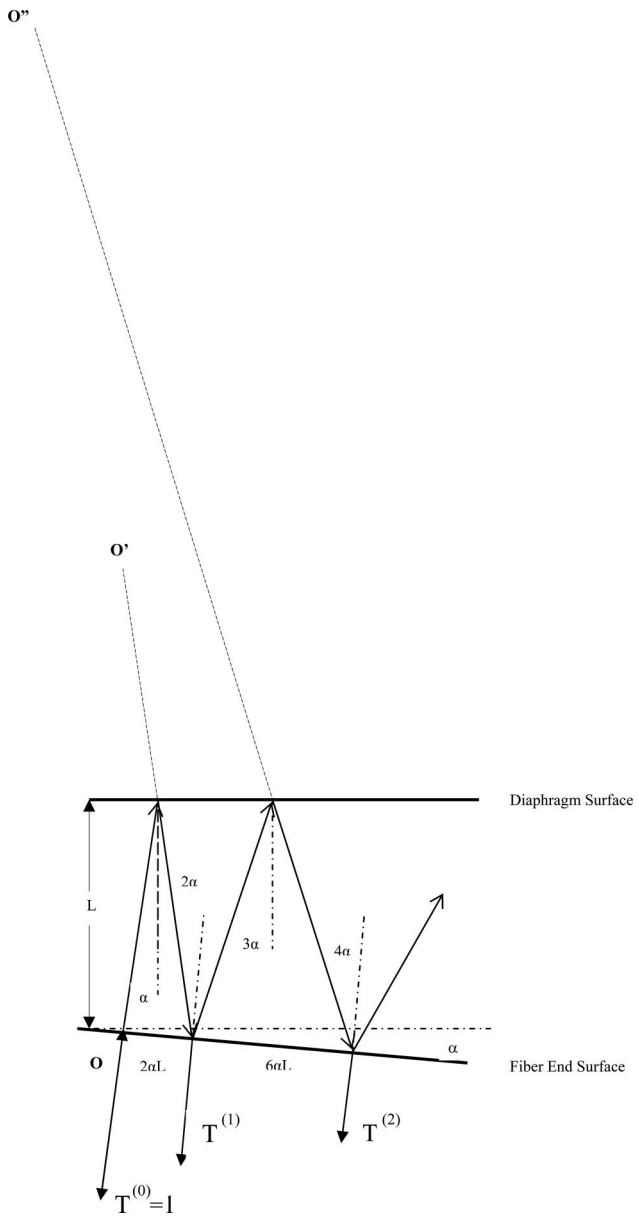

Fig. 4. Fiber coupling coefficients calculated from image sources.

we take into account the fiber coupling efficiency (or loss) for a DFOS, Eq. (1) must be replaced by

$$E^{(r)} = r + \sqrt{T^{(1)}}tt'r''e^{i2\phi} + \sqrt{T^{(2)}}tt'r''e^{i2\phi}(r'r''e^{i2\phi}) + \sqrt{T^{(3)}}tt'r''e^{i2\phi}(r'r''e^{i2\phi})^2 + \cdots, \tag{33}$$

where both ϕ (phase interference) and $T^{(m)}$ (intensity coupling coefficient) are L dependent and can serve as the mechanisms of sensor application. No finite expression for $I^{(o)}/I^{(t)}$ similar to Eq. (3) or Eq. (7) can be derived from Eq. (33), since $T^{(m)}$ is far from being a geometric series.

Apparently, to make a pure Fabry–Perot DFOS, both L and α must be extremely small. For example, when $L = 2$ μm, under the conditional $\alpha = 0$, we have

$T^{(1)}$, $T^{(2)}$, and $T^{(3)}$ all >0.99, and Eq. (33) is reduced to Eq. (1). The DFOS can be treated as a plane wave Fabry–Perot interferometric device following Eqs. (3) and (7). On the other hand, witht the same L = 2 μm, but α = 0.5°, we have $T^{(1)}$ = 0.9384, $T^{(2)}$ = 0.7738, and $T^{(3)}$ = 0.5571. It is not appropriate to characterize the DFOS as following Eq. (1).

So far most of the reported work on DFOS has $L > 60$ μm. With or without α, $T^{(m)}$ is far from 1. For example, when L = 90 μm and α = 0.5°, we have $T^{(1)}$ = 0.3010, $T^{(2)}$ = 0.0638, and $T^{(3)}$ = 0.0139. Note that $T^{(2)}$, $T^{(3)}$, . . . are all negligible in comparison with $T^{(1)}$. Also note that $T^{(1)}$ is L dependent. Thus it seems more appropriate to classify such a DFOS as a mixture of two mechanisms based on two-beam interference as well as intensity coupling.

3. Preliminary Experimental Results of a Diaphragm Fiber-Optic Sensor

Experimentally, we have designed a DFOS with interference gap width L as narrow as 2 μm and diaphragm fiber angular misalignment as small as 0.1°. To meet such strict design demands, microelectromechanical system (MEMS) technology was used, and a special precision diaphragm fiber assembling tool was also utilized. Figure 5 is the design of the MEMS DFOS. For Q-point stabilization, microchannels were incorporated into the design. Figure 6 is an optical micrograph of the processed diaphragm of the Q-point stabilized MEMS DFOS.

Because the effects of multiple beam interference and intensity coupling coefficient variation are mixed and nonseparable as shown in Eq. (33), it is proposed that to confirm a DFOS that functions as a Fabry–Perot interferometric device a critical test of $I^{(o)}/I^{(t)}$ versus static pressure P or gap width L be performed over more than one period to verify if the fabricated DFOS satisfies Eq. (3). Figure 7 is the experimental result of such a test of our new DFOS. Note that, to

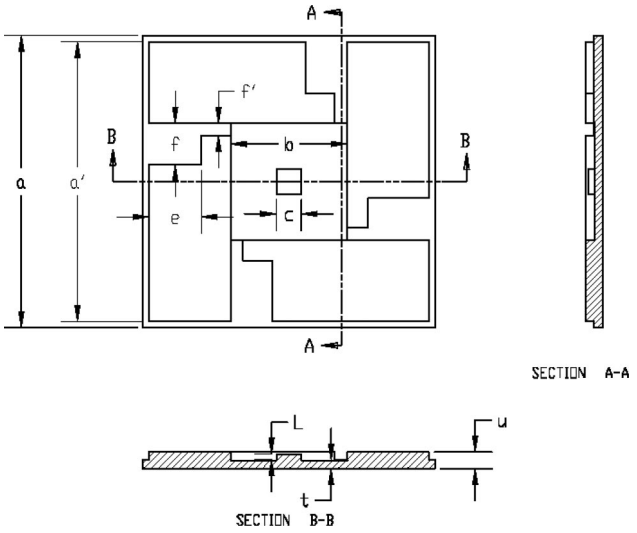

Fig. 5. DFOS with the design of the Q-point stabilized by microchannels.

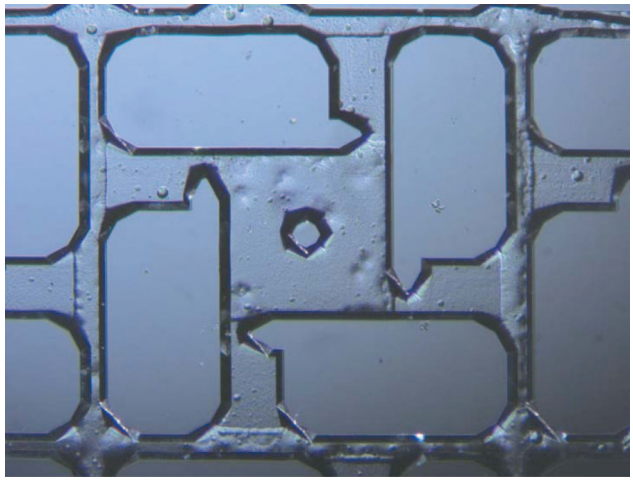

Fig. 6. (Color online) Optical microscope image of the fabricated Q-point stabilized DFOS showing an embossed center and microchannels.

the best of our knowledge, such an experiment has never before been successfully performed. Also note that this is the first DFOS that has such a narrow gap width and precision fiber angular alignment and passes the critical test to satisfy Eq. (3) as a purely Fabry–Perot interferometric device.

We emphasize that the current practice of using dynamic characterization cannot distinguish the Fabry–Perot DFOS from two-bean interference DFOS, or DFOS based on a mixture of interference and intensity effects, or a purely intensity-based DFOS, since all the above types of DFOS have a dependence of $I^{(o)}/I^{(t)}$ on P, and therefore can be utilized for acoustic or dynamic pressure sensing. Another widely used technique of characterization of such a device is the use of a wavelength instead of pressure as the variable to demonstrate the interference effect. Such a method shows only the interference effect but fails to show the lack of a coupling coefficient variation with the deflection of the diaphragm, which is the basis of intensity-based fiber-optic devices.

Our DFOS samples that passed the rigorous static pressure test were characterized as an audible mi-

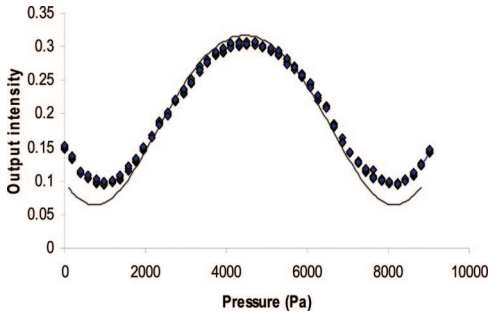

Fig. 7. (Color online) Static characterization of output optical intensity $I^{(out)}/I^{(in)}$ as a function of pressure in comparison with the calculated curve from Eq. (10). Note that the contrast of the experimental result is not as strong as the calculated data because of the scattering and other noise-generating mechanisms.

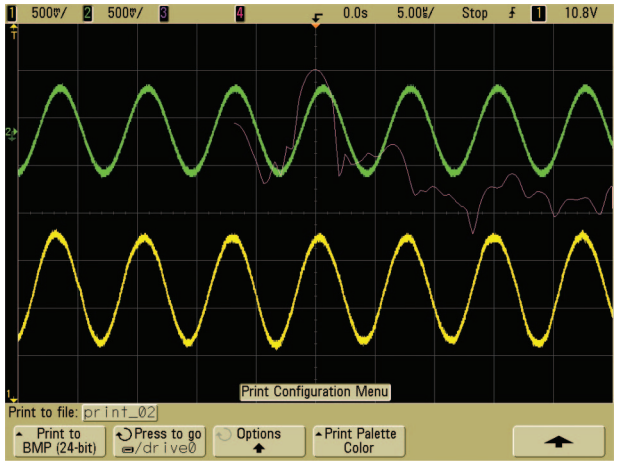

Fig. 8. (Color online) Comparison of the DFOS and the PZT as hydrophones: green (upper), PZT from the PAC; yellow (lower), DFOS of the NJIT and the PSEG; red (thin curve), FFT of the input signal peaked at 150 kHz.

crophone used in the air and as a hydrophone in the 150 kHz range. When used as a microphone, the human voice is accurately reproduced without excessive noise. Therefore, the widely used but cumbersome technique of signal modulation and demodulation is not needed. The detailed results of the microphone's characterization will be reported elsewhere [16]. Functioning as an ultrasonic hydrophone, our DFOS is placed side by side with a commercial piezoelectric transducer (PZT) acoustic sensor manufactured by the Physical Acoustics Corporation [(PAC) Princeton Junction, New Jersey]. Figure 8 compares the detected acoustic signal of our DFOS with that of the PZT. Again no modulation and demodulation of the acoustic signal are used, neither are the noise or bandwidth reducing filters. Both the DFOS and the PZT sensors are at the same distance from a 150 kHz acoustic signal generated by a PAC PZT transducer. Performance of the new Fabry–Perot DFOS in terms of sensitivity, dynamic range, and harmonic distortion is virtually identical with that of the commercial PZT [16] sensor.

4. Summary and Discussion

In summary, the theory of a diaphragm fiber optic sensor has been proposed. A pure interference-based Fabry–Perot DFOS designed with an extremely narrow interference gap width and precision diaphragm fiber alignment and fabricated with MEMS technology, has been demonstrated for the first time, to the best of our knowledge. By modifying the fiber endface with an antireflection coating and diaphragm with a 100% reflecting gold coating, the DFOS can also be used as a fiber-optic mirror to replace the bulk mirror that is used for fiber-optic Michelson interferometric devices. The excellent performance of the newly demonstrated DFOS, with its small size, low cost, flexible installation, high sensitivity, and convenience for multiplexing and integration, can lead to a broad range of new applications.

The authors acknowledge helpful discussions with S. Hsu, H Ou, and I. Padron. The research was partly supported by the Public Service Enterprise Group (PSEG) Power LLC and Foundation of the New Jersey Institute of Technology (NJIT).

References

1. A. Wang, Y. Liu, and B. Ward, "Prototype fiber-optic acoustic partial discharge sensor: lessons-learned documentation and field test," Tech. Rep. 1001768 (Electric Power Research Institute, 2002).
2. B. Yu, D. W. Kim, J. Deng, H. Xiao, and A. Wang, "Fiber Fabry–Perot sensors for detection of partial discharges in power transformers," Appl. Opt. **42,** 3241–3250 (2003), and references therein.
3. M. Yu and B. Balachandran, "Acoustic measurements using a fiber optic sensor system," J. Intell. Mater. Syst. Struct. **14,** 409–414 (2003).
4. A. Saran "MEMS based Fabry–Perot pressure sensor and non-adhesive integration on optical fiber by anodic bonding," Ph.D. dissertation (University of Cincinnati, 2004).
5. S. Wang, B. Li, Z. Xiao, S. H. Lee, H. Roman, O. L. Russo, K. K. Chin, and K. R. Farmer, "An ultra-sensitive optical MEMS sensor for partial discharge detection," J. Micormech. Microeng. **15,** 521–527 (2005).
6. J. Xu, G. Pickrell, X. Wang, W. Peng, K. Cooper, and A. Wang, "A novel temperature-insensitive optical fiber pressure sensor for harsh environments," IEEE Photon. Technol. Lett. **17,** 870–872 (2005).
7. Y. Zhu and A. Wang, "Miniature fiber-optic pressure sensor," IEEE Photon. Technol. Lett. **17,** 447–449 (2005).
8. C. Fabry and A. Perot, "Théorie et applications d'une nouvelle méthode de Spectroscopie Interferentielle," Ann. Chim. Phys. **16,** 115–144 (1899).
9. M. Born and E. Wolf, *Principles of Optics,* 6th ed. (Pergamon, 1980), p. 327.
10. S. Timoshenko, *Strength of Materials, Part 2,* 3rd ed. (Van Nostrand, 1983), p. 97.
11. M. di Giovanni, *Flat and Corrugated Diaphragm Design Handbook* (Marcel Dekker, 1982).
12. B. E. A. Saleh and M. C. Teich, *Fundamentals of Photonics* (Wiley–Interscience, 1991).
13. A. Yariv, *Optical Electronics,* 4th ed. (Holt, Rinehart & Winston, 1991).
14. D. Marcus, "Loss analysis of single-mode fiber splices," Bell Syst. Tech. J. **56,** 703–718 (1977).